Nanoscale

RSC Publishing

PAPER

Two-photon excited fluorescence of silica nanoparticles loaded with a fluorene-based monomer and its cross-conjugated polymer: their application to cell imaging†

Cite this: *Nanoscale*, 2012, 4, 7751

Laura Aparicio-Ixta,[a] Gabriel Ramos-Ortiz,*[a] Juan L. Pichardo-Molina,[a] José Luis Maldonado,[a] Mario Rodríguez,[a] Víctor M. Tellez-Lopez,[b] Daniel Martinez-Fong,[bc] Mikhail G. Zolotukhin,[d] Serguei Fomine,[d] Marco. A. Meneses-Nava[a] and Oracio Barbosa-García[a]

In this work the two-photon activity of nanoparticles obtained from a fluorene monomer (**M1**) and its cross-conjugated polymer (**P1**) is reported. Aqueous suspensions of **M1** and **P1** nanoparticles prepared through the reprecipitation method exhibited maximum two-photon absorption (TPA) cross-sections of 84 and 9860 GM (1 GM = 10^{-50} cm^4 s) at 740 nm, respectively, and a fluorescence quantum yield of ~1. Such a two-photon activity was practically equal with respect to that for molecular solutions of **M1** and **P1**. These materials were then successfully encapsulated into silica nanoparticles to provide biocompatibly. A lung cancer cell line (A549) and a human cervical cancer cell line (HeLa cells) were incubated with our fluorescent silica nanoparticles to carry out two-photon imaging. By means of these studies we demonstrate that optimized nonlinear optical polymers loaded in silica nanoparticles can be used as efficient probes with low cytotoxicity and good photostability for two-photon fluorescence microscopy. To the best of our knowledge, studies concerning polymer-doped silica nanoparticles exhibiting large two-photon activity have not been reported in the literature.

Received 18th July 2012
Accepted 13th October 2012

DOI: 10.1039/c2nr31925j

www.rsc.org/nanoscale

Introduction

Organic molecules and polymers that exhibit an efficient TPA process have attracted increasing attention in relation to some applications such as two-photon laser scanning microscopy,[1] optical power limiting,[2] 3-D microfabrication,[3] data storage[4] and photodynamic therapy.[5] Among these applications, two-photon laser scanning microscopy has gained great acceptance in the biomedical community as a tool to provide direct observation of cellular structure and biological processes. This microscopy offers several advantages over traditional techniques such as higher resolution, higher depth penetration in tissue, more reduction of photobleaching and weak autofluorescence.

Nevertheless, it should be pointed out that commercially available organic fluorophores currently used in two-photon imaging exhibit very small TPA with cross-sections commonly in the range of 1–100 GM (1 GM = 10^{-50} cm^4 s).[6,7]

Intensive investigations during the last two decades have produced several reports on organic materials possessing high TPA properties,[8,9] however, the toxicity of the organic solvents in which they are soluble greatly limits their applications in the two-photon imaging technique. To circumvent these limitations, nanoscience has recently provided methods to bring organic molecules into biological media such as water. For instance, following such methods aqueous suspensions of organic nanoparticles,[10,11] dye-loaded latex spheres[12,13] and dye-doped silica nanoparticles[14–16] can be synthesized. Among these approaches the latter results are particularly attractive, since silica encapsulation of organic dyes provides good optical transparency, chemical and thermal stability, low cytotoxicity, and inertness to the environment.[15] In addition, silica nanoparticles can be surface-functionalized with various types of chemical groups for conjugation with different targeting bio-molecules.

Conjugated polymers have also been employed for the synthesis of nanoparticles.[17–19] The advantage of employing this type of polymers as fluorescent probes is that they comprise TPA cross-sections between two to three orders of magnitude larger compared with common dyes, and also exhibit low levels of aggregation-induced fluorescence quenching. It is worth mentioning that in spite of these advantages, silica encapsulation of conjugated polymers to obtain luminescent

[a]*Centro de Investigaciones en Óptica A.C., A.P. 1-948, 37000 León, Gto., Mexico. E-mail: garamoso@cio.mx; Fax: +52 (477) 441 42 09; Tel: +52 (477) 441 42 00*

[b]*Departamento de Fisiología, Biofísica y Neurociencias, CINVESTAV, Apdo. Postal 14-740, 07000 México, D.F., Mexico*

[c]*Programa de Doctorado en Nanociencias y Nanotecnología, CINVESTAV, Apdo. Postal 14-740, 07000 México, D.F., Mexico*

[d]*Instituto de Investigaciones en Materiales, Universidad Nacional Autónoma de Mexico, Apartado Postal 70-360, CU, Coyoacán 04510, México D. F., Mexico*

† Electronic supplementary information (ESI) available. See DOI: 10.1039/c2nr31925j

nanoparticles has not been fully investigated, and attention has focused on the synthesis of dye-doped silica nanoparticles.[20–22] Very few examples of polymer-loaded silica nanoparticles can be cited from the literature. For instance, Tan *et al.*[23] demonstrated the integration of conjugated polymers and superparamagnetic iron oxide nanocrystals into silica nanocapsules, while Wu *et al.*[19] suggested silica encapsulation of the very well known conjugated polymer MEH-PPV as a strategy to facilitate biofunctionalization. In these examples, however, the nonlinear optical properties of nanoparticles were not explored. The aim of the present work is then to explore optical nonlinearities of polymer-loaded silica nanoparticles and their use in two-photon imaging.

Here we report on the fabrication and TPA properties of aqueous suspensions of silica nanoparticles loaded with a fluorene-based cross-conjugated polymer (**P1**). The results are compared with those obtained from dye-loaded silica nanoparticles, this dye being the monomer (**M1**) of such a conjugated polymer. Fig. 1 shows the molecular structures of these two organic compounds. Our study also includes the TPA properties of organic solutions of **M1(P1)** and aqueous suspensions of nanoparticles of **M1(P1)** without silica encapsulation. The fluorene-based compounds used in this study belong to a family of materials that have been extensively used in organic electronics for applications such as electroluminescent devices (OLEDs) and photovoltaic cells (OPVs).[24,25] They are also of great interest in nonlinear optics because they possess improved third-order nonlinear characteristics including TPA.[8,9,26–28]

In the case of **P1**, we recently reported large third-order nonlinear susceptibilities measured through coherent frequency conversion experiments within the telecommunication wavelength range 1100–1600 nm.[29] In continuation to those studies, the present work demonstrates that **P1** also possesses excellent TPA activity at wavelengths of biomedical interest. That is, **P1** exhibits enhanced nonlinear absorption in the wavelength range of 740–820 nm and high quantum yield of fluorescence. Furthermore, such properties are conserved either after agglomeration to form polymer nanoparticles or after encapsulation into silica nanoparticles. The nanoparticles so obtained were then tested on A549 and HeLa cell lines to obtain images through two-photon laser scanning microscopy.

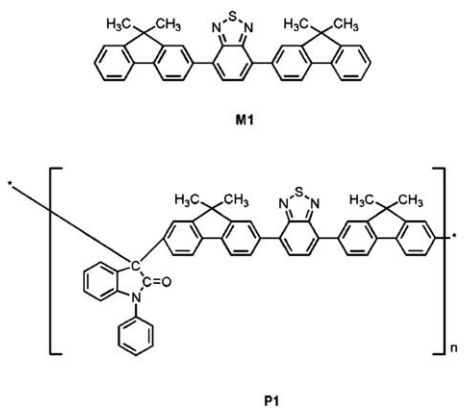

Fig. 1 Chemical structures of the fluorene monomer **M1** and its cross-conjugated polymer **P1**.

Experimental section

Materials

The synthesis of the fluorene monomer 4,7-bis[2-(9,9-dimethyl) fluorenyl]benzo[1,2,5]thiadiazole (**M1**) and its cross-conjugated polymer (**P1**) was reported elsewhere.[29] According to GPC data, the molecular weights M_w and M_n of **P1** are 1.22×10^5 and 8.47×10^4 g mol^{-1}, respectively. For the synthesis of organic nanoparticles and doped silica nanoparticles the following chemicals were utilized: deionized water, 1-butanol 99.8%, 1-sodium bis(2-ethylhexyl)sulfosuccinate (Aerosol-OT), *N*-methyl-2-pyrrolidinone (NMP), triethoxyvinylsilane (VTES), 3-aminopropyltriethoxysilane (APTES) and 3-(trihydroxysilyl)propyl methylphosphonate monosodium salt solution (THPMP), tetrahydrofuran (THF), hexadecyltrimethyl-ammonium bromide (CTAB), *p*-(1,1,3,3-tetramethylbutyl) phenoxypolyoxyethylene glycols (Triton X-100) and albumin. All these chemicals were purchased from Sigma Aldrich. Cell-culture products and Hoechst 33258 were purchased from GIBCO™ (Invitrogen Corporation, Grand Island, NY).

Theoretical methods

The transition energies for low lying excited states in **M1** and **P1** were calculated using time dependent implementation of density functional theory (DFT). CAM-B3LYP functional specially designed for electronic spectra simulation has been used in conjunction with 6-31++G(d,p) basis set.[30] A SMD solvation model was applied as implemented in Gaussian 09 suite of programs using THF as a solvent.[31] The geometry of **M1** and **P1** was optimized to a global minimum at M06-2X/6-31G(d) level in THF using the SMD solvation model.

Fabrication of organic nanoparticles by the reprecipitation method

The reprecipitation method was employed to prepare nanoparticles of **M1** (**M1**-NPs) and **P1** (**P1**-NPs). First, 1 mg of these materials was dissolved in 2 mL of THF. Then a small volume of these solutions (typically in the range 0.25–0.8 mL) was injected quickly and under sonication in 8 mL of deionized water or in 8 mL of aqueous solution containing one of the following surfactants: CTAB, Triton X-100 or albumin. The surfactants were used at concentrations in the range of 0.08–0.8 mM to achieve high nanoparticles concentration and long stability. THF was then removed by evaporation under vacuum, followed by filtration through membrane filters with 0.2 μm cutoff. The resulting aqueous suspensions of nanoparticles were of high optical quality and without significant light scattering.

Synthesis of M1 and P1 doped silica nanoparticles

Doped silica nanoparticles were synthesized based on methods described by Wang *et al.*, Qian *et al.*, and Arriagada *et al.*[32–34] The process consists of the preparation of a microemulsion system to synthesize silica nanoparticles (SNPs) in the nonpolar core of Aerosol-OT/1-butanol micelles in water. Micelles were prepared by dissolving either 0.22 g or 0.44 g of Aerosol-OT, 300 μL of 1-butanol and 200 μL of NMP in 10 mL of deionized water by

magnetic stirring. NMP was used as a hydrophilic solvent for **M1(P1)** and exhibits unlimited water miscibility. Then, 200 μL of **M1** or **P1** dissolved in NMP at the concentration of 10 mM and 0.1 mM, respectively, was added to the micellar solution under constant magnetic stirring. Half an hour later, 100 μL of neat VTES was added to the micellar system, and the resulting solution was stirred for about 1 h. Next, the doped **M1** and **P1** silica nanoparticles (**M1**-SNPs and **P1**-SNPs, respectively) were precipitated by adding 20 μL of APTES or THPMP and stirring the solution for 20 h at room temperature. The use of two different precursors such as APTES or THPMP allowed us to modify the surface of SNPs with amine groups (NH_2) or methyl phosphonate groups ($MePO_2^-$), respectively. To remove surfactants, co-surfactants, non-encapsulated **M1(P1)** and residues of unreacted precursors, the suspension was dialyzed against deionized water in a 8–10 kDa cutoff cellulose membrane Float-A-Lyzer G2 for 72 h. Aqueous suspensions of **M1**-SNPs and **P1**-SNPs were obtained at different concentrations and special care was taken to eliminate big particles by filtering the suspensions with a membrane filter with 0.2 μm cutoff. The resultant samples exhibited high colloidal stability.

Two-photon excited fluorescence experiments and fluorescence quantum yield

Two-photon absorption cross-section of samples was measured through the two-photon excited fluorescence (TPEF) technique[35] using a Ti:sapphire laser (100 fs per pulse, repetition rate of 80 MHz, tunability 740–820 nm). The laser beam was focused into a quartz cell of 1 cm path length (containing the samples) by using a 5 cm focal-length lens. The TPEF emission was collected using a lens in an epi-illumination configuration (in a perpendicular direction with respect to the excitation beam) and focused into the input slit of a spectrometer. The fluorescence quantum yield of samples at low concentrations ($<1 \times 10^{-5}$ mol L^{-1}) was determined by using the integrating sphere method with excitation provided by a diode laser operating at 375 nm. In this case, the laser dye Rhodamine 6G was used as a standard while for TPEF experiments Rhodamine 6G and Rhodamine B were independently employed as standards. The quantum yield and two-photon absorption cross-sections of these standards have been recently fully characterized.[36]

Cell culture

HeLa (cell line derived from cervical cancer) and A549 (cell line derived from lung adenocarcinoma) cells were cultivated in Dulbecco's minimum essential media (DMEM) with 10% fetal bovine serum (FBS), 1% penicillin–streptomycin solution and 2 mM glutamine at 37 °C in an atmosphere with 5% CO_2 until a confluence of 70–80%. Then the cells were washed thrice with phosphate-buffered saline (1× PBS). After fixation with 4% paraformaldehyde, the fluorescent samples (**M1**-NPs, **P1**-NPs, **M1**-SNPs or **P1**-SNPs) were added and the cells were incubated for 1 h at room temperature away from light. Then the volume was removed and the cells were washed once with 1× PBS. Cell nucleus was stained with 1 μM of Hoechst 33258. Finally the cells were imaged through a Leica TCS-SP5 MP two-photon laser scanning microscope (Leica Microsystem, Wetzlar Germany).

Cell cytotoxicity assay

Methylthiazolyldiphenyl-tetrazolium (MTT) assays were performed to assess the cytotoxicity of fluorescent samples in HeLa and A549 cells. These cells were seeded in 96-well plates and incubated at 37 °C with 5% CO_2 for 24 h to allow adherence to the well. Then dilutions (in the range 1 : 1 to 1 : 32) of the aqueous suspensions of **M1(P1)**-NPs, **M1(P1)**-SNPs in DMEM medium were made and the cells were incubated for 24 h to allow the suspensions of nanoparticles to act on all cells. After this, the medium was removed and replaced with fresh culture medium. Next, MTT (0.5 mg mL^{-1}) in 1× PBS solution was added into each well. The MTT medium solution was carefully removed after 4 h of incubation and purple MTT-formazan crystals were formed. Finally, this precipitate was dissolved by adding isopropanol and the absorbance of MTT at 540 nm was measured by an ELISA microplate reader (Labsystems Multiskan). The percentage of viability was obtained as follows: % viability = OD treated cells × 100/OD control cells.

Results and discussions

Linear absorption

Fig. 2a shows the UV-vis absorption spectra from THF solution of **M1** (**M1**-THF) and from aqueous suspensions of nanoparticles of **M1** (**M1**-NPs) and **M1**-doped silica nanoparticles (**M1**-SNPs). Two absorption bands are present in these spectra.

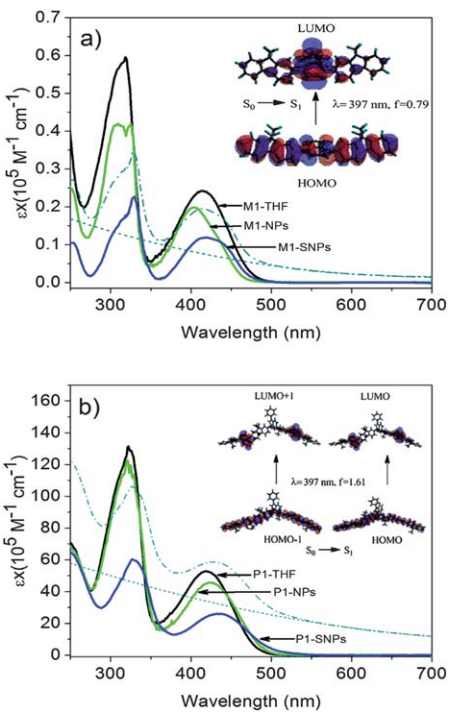

Fig. 2 Linear absorption spectra from (a) THF solution of **M1**, aqueous suspensions of **M1**-NPs and aqueous suspensions **M1**-SNPs; (b) THF solution of **P1**, aqueous suspensions of **P1**-NPs and aqueous suspensions **P1**-SNPs. In the case of **M1(P1)**-NPs the suspensions are stabilized with CTAB. The dash-dotted line represents the **M1(P1)**-SNPs absorption spectrum before scattering subtraction and the dotted line the scattering baseline. Insets: molecular orbitals showing the ICT character in $S_0 \rightarrow S_1$ transitions calculated for models of **M1** and **P1**.

Our calculations performed within the framework of DFT for a model of **M1**-THF showed that the long wavelength absorption maxima ($S_0 \rightarrow S_1$) at 415 nm are due to a significant intramolecular charge transfer (ICT) process, where the charge is transferred from π orbitals of fluorene fragments to π^* orbitals of benzothiadiazole (charge density distribution for the HOMO and LUMO orbitals is displayed in the inset of Fig. 2a and in the ESI, Fig. S1†). In the case of **M1**-NPs it is observed that the π–π^* transition (404 nm) is blue-shifted compared with **M1**-THF. Commonly, blue shifting is assigned to molecular bending or to a decrease in the Stokes shift that results from restraint of vibronic relaxation, as it has been observed by other authors who reported on organic nanoparticles in mixtures of solvent and water.[10] In our case, however, the use of surfactants to stabilize nanoparticles in water plays a role in localization of the absorption peak. For instance, nanoparticles stabilized with CTAB and Triton X-100 produced a blue shifting of 9 nm as compared with THF solution, but a red shifting of 8 nm was detected when albumin was employed as the surfactant (result not included in Fig. 2). In regard to **M1**-SNPs the peak of maximum absorption did not display significant shifting with respect to **M1**-THF. The presence of silica nanoparticles, however, is clearly evident in absorption spectra since they produce light scattering, *i.e.*, the real absorption bands are superimposed onto a baseline of scattering. The so obtained absorption spectra from **M1**-SNPs were the same independent of the silane-based precursors (APTES or THPMP) utilized during their synthesis. To correct the absorption spectra and remove the scattering artifact shown in Fig. 2, we used the empirical approach followed by Lebret *et al.*[37] Thus, the region of null absorption of **M1**, from 550 to 700 nm, was used as the model of the baseline that is extrapolated to shorter wavelengths through a polynomial regression. A good approximation of the real absorption spectrum was then obtained by subtracting the scattering baseline from the measured spectrum.

Fig. 2b displays the UV-vis absorption spectrum from a THF solution of **P1** (**P1**-THF). Similar to the case of **M1**, our DFT calculations demonstrated that absorption at long wavelengths in **P1**-THF is also dominated by the ICT character. In this case the optical properties of the polymer were simulated by using an oligomer as a model (see ESI Fig. S2†). We can observe that four molecular orbitals are involved in $S_0 \rightarrow S_1$ transition (HOMO-1, HOMO, LUMO, LUMO+1). Such a π–π^* transition appears at 419 nm in **P1**-THF but it is red-shifted to 423 and 435 nm for **P1**-NPs and **P1**-SNPs (independent of the use of APTES or THPMP as a silane-based precursor), respectively. Comparable red-shifting has been observed previously in nanoparticles synthesized from fluorene polymers[17] although other authors have reported a blue-shifting effect in similar compounds.[19] The discrepancy between these observations is ascribed to the specific structure of the utilized hydrophobic polymer and the conformational changes introduced in the structure when it is brought in an aqueous environment.

Transmission electron microscopy

Our nanoparticles were analyzed through transmission electron microscopy (TEM). The size and dispersion of nanoparticles were determined by parameters used during the synthesis such as the concentrations of surfactants, organic materials, and silica precursors. Our attention was focused on nanoparticles obtained from **P1**. For instance, Fig. 3a and b present micrographs of **P1**-NPs from suspensions (4.1×10^{-7} M) processed with two different concentrations of CTAB (0.08 and 0.8 mM, respectively). The mean sizes of **P1**-NPs so obtained were 29 nm and 19 nm, respectively. As expected, higher concentration of surfactant reduced the nanoparticles size. Likewise, for the case of **P1**-SNPs different sizes were obtained from suspensions (3.1×10^{-7} M) by varying the amount of aerosol-OT utilized during their synthesis. Fig. 3c and d present **P1**-SNPs with mean sizes of 125 nm and 40 nm obtained with two different concentrations of aerosol-OT (50 mM and 98 mM, respectively). From these TEM micrographs it is clearly observed that the reprecipitation method produced **P1**-NPs with irregular shapes while silica encapsulation produced **P1**-SNPs with spherical shape. The insets of Fig. 3 show the nanoparticles size distribution obtained from the analysis of various TEM micrographs. We performed additional experiments to obtain NPs size distribution through dynamic light scattering (DLS). In this case, the size of nanoparticles was in relatively good agreement with TEM results, although the mean sizes were somewhat larger and with broader size distribution. For instance, suspension of **P1**-NPs processed with CTAB at a concentration of 0.08 mM (Fig. 3a) resulted in a mean size of 41 nm, while **P1**-SNPs synthesized with aerosol-OT at a concentration of 50 mM (Fig. 3c) resulted in a mean size of 154 nm (see Fig S3†).

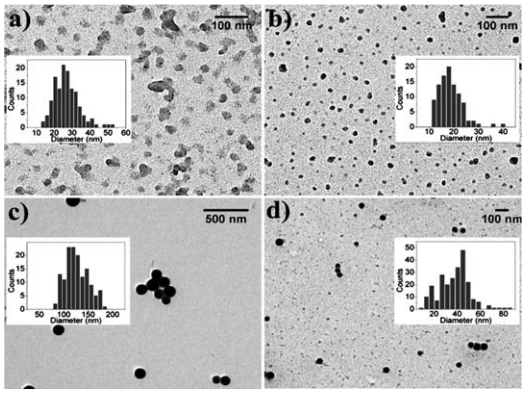

Fig. 3 TEM micrographs of **P1**-NPs obtained from suspension processed with two different concentrations of CTAB: (a) 0.08 mM and (b) 0.8 mM. TEM micrographs of **P1**-SNPs obtained with two different concentrations of aerosol-OT: (c) 50 mM and (d) 98 mM. Insets: nanoparticles size distribution from the analysis of various TEM micrographs.

Photoluminescence properties

One-photon excited fluorescence (OPEF) spectra from monomer **M1** and cross-conjugated polymer **P1** in solutions and aqueous suspensions are displayed in Fig. 4. Emission spectra undergo wavelength shifting for the case of nanoparticles. In particular, the monomer **M1** exhibited notorious changes such that the emission peaks in **M1**-NPs and **M1**-SNPs were blue-shifted approximately 5 nm and 16 nm, respectively, compared with the

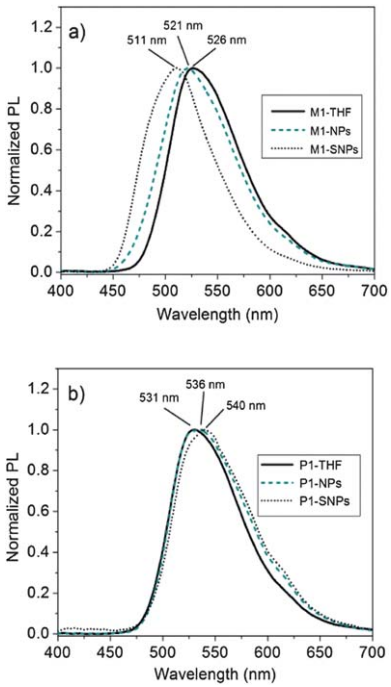

Fig. 4 Normalized photoluminescence (PL) spectra for (a) monomer **M1** and (b) polymer **P1** in solutions and aqueous suspensions. Excitation: UV lamp.

peak of **M1**-THF. In contrast, fluorescence peaks of **P1**-NPs and **P1**-SNPs exhibited red-shifting of 4 nm and 9 nm, respectively. Thus, the changes in the energies corresponding to the π–π* transition in the absorption spectra shown in Fig. 2 are consistent with the wavelength shifts observed in photoluminescence spectra shown in Fig. 4.

Fluorene based molecules and polymers are recognized for exhibiting high quantum yields (ϕ) of fluorescence. Our measurements through the integrating sphere method demonstrated that both **M1** and **P1** in dilute THF solutions have values of $\phi \sim 1$, in agreement with the values for similar fluorene compounds reported by other authors.[32,38,39] The integrating sphere method was also applied to aqueous suspensions under study in order to know to what extent ϕ is affected due to the introduction of channels of non-radiative decays for excited states when **M1(P1)** is agglomerated or loaded into silica nanoparticles. Table 1 summarizes the results. For these measurements concentrations of aqueous suspensions were kept below 1×10^{-5} mol L^{-1}. Notoriously, both **M1**-NPs and **P1**-NPs did not exhibit strong effects of photoluminescence quenching and the quantum yields remained close to one, although for the case of **M1**-SNPs and **P1**-SNPs there was a reduction of about 30% and 25%, respectively. Despite the photoluminescence quenching exhibited by **M1**- and **P1**-loaded silica nanoparticles, the obtained values for ϕ are comparable with those exhibited by some representative fluorescent nanoparticles reported recently, *i.e.*, organically modified silica nanoparticles entrapping fluorene dyes ($\phi = 0.49$)[32] and polymeric nanocarriers encapsulating aggregation-induced emission (AIE) dyes ($\phi = 0.62$).[40] For these examples as well as for our nanoparticles, ϕ resulted in considerably much larger yields than most of the quantum yields reported in seminal works on nanoparticles of conjugated polymers.[18,19]

Table 1 Wavelengths of maximum absorbance and fluorescence, quantum yield and maxima TPA cross-sections

Sample	Absorbance λ_{max} (nm)	Fluorescence λ_{max} (nm)	ϕ	σ^{TPA} (max) (GM)
M1-THF	415	526	~1	84
M1-NPs	404	521	~1	72
M1-SNPs	415	511	0.7	76
P1-THF	419	531	~1	9860
P1-NPs	423	536	0.95	8481
P1-SNPs	435	540	0.75	8686

Two-photon absorption

M1 and **P1** in THF solutions and aqueous suspensions of **M1**-NPs, **M1**-SNPs, **P1**-NPs and **P1**-SNPs emit intense upconverted fluorescence under infrared excitation within the tunability of the Ti:sapphire laser (740–820 nm). We verified the nature of the fluorescence induced by femtosecond pulses at 800 nm by measuring its intensity as a function of the input laser power; a nearly quadratic dependence confirmed that the nature of the upconverted fluorescence was indeed induced by two-photon absorption (see insets in Fig. 5). For all samples, the TPEF spectra (see Fig. S4†) were the same compared with the OPEF spectra shown in Fig. 4, indicating that in both cases the light emission originated from the same lowest lying transition in the singlet

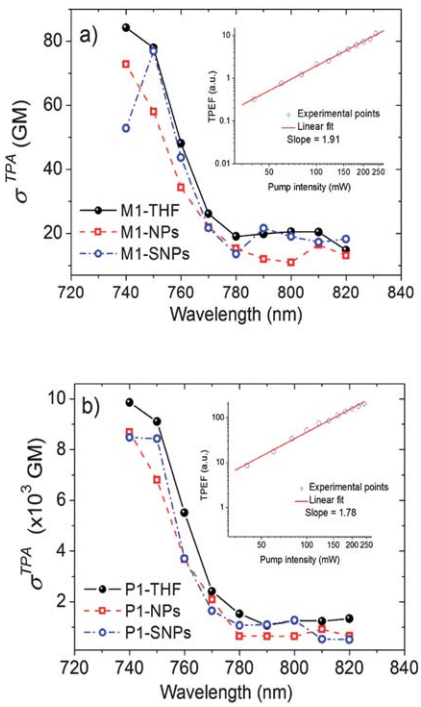

Fig. 5 Two-photon absorption spectra of (a) **M1** and (b) **P1** in solutions and aqueous suspensions of nanoparticles and loaded silica nanoparticles. Insets: log–log plots for the dependence of TPEF on pump intensity for **M1**-SNPS and **P1**-SNPs.

manifold. Fig. 5 shows the two photon-absorption cross-sections (σ^{TPA}) as a function of the excitation wavelength for all samples. We point out that the measured values of σ^{TPA} were practically the same when Rhodamine 6G or Rhodamine B were employed as standards in our TPEF experiments, in spite of their σ^{TPA} values and quantum yields differing appreciably.[36] This confirmed that our experimental setup was well calibrated. For all samples the nonlinear absorption increases at shorter wavelengths (within the range of tunability of the excitation source). The maximum σ^{TPA} was obtained at 740 nm for **P1**-THF with a value of approximately 9.8×10^3 GM. This is a 117-fold increment with respect to the maximum nonlinearity measured for **M1**-THF. We see that this increment is in correspondence with the number of repeating units in **P1** (see molecular weights M_w and M_n for **P1** in the Experimental section), and in consequence the large nonlinearity of **P1** is due to an additive effect of the nonlinearities from individual units, *i.e.*, the σ^{TPA} values per repeating unit are similar to that exhibited by **M1**. As it was explained previously, **M1** and **P1** exhibit an ICT character upon excitation, such that the charge is transferred from fluorene fragments located at the edges of each monomer/polymer section to the central benzothiadiazole moiety (see Fig. 1). This means that the nonlinear response of **M1** and **P1** is of quadrupolar origin.

Notice from Fig. 5 that nonlinearities from **M1** and **P1** measured in THF solutions are not substantially affected when such materials agglomerate to form nanoparticles or when they are encapsulated into silica nanoparticles. It should be mentioned that the optical properties of aqueous suspensions of bare nanoparticles synthesized through the reprecipitation method without the use of surfactants were also studied and gave similar results to those of **M1**-NPs and **P1**-NPs prepared with the use of surfactants such as CTAB and Triton X-100, but they lacked a desirable stability for long periods and in general generated suspensions with lower nanoparticle concentrations. Similarly, in the case of **M1**-SNPs and **P1**-SNPs the measured σ^{TPA} values were independent of the silane-based precursors (APTES or THPMP) and the amount of surfactants utilized during their synthesis. There are many examples of silica nanoparticles loaded with organic dyes[15,20–22] in the literature and recently attention has focused on nanoparticles loaded with dyes exhibiting enhanced TPA.[16,19,33,37,41] However, to the best of our knowledge, **P1**-SNPs are the first example of polymer-loaded silica nanoparticles intended for two-photon activity. The use of a polymer to be loaded into silica nanoparticles represents an advantage in terms of low fluorescence quenching and high nonlinearities, as in the case of **P1** whose two-photon activity is between two and three orders of magnitude higher than in common dyes and other representative materials.[25,26] It should be emphasized that such high nonlinearities in the cross-conjugated polymer **P1** are based on the additive effect of repeating units, as it is observed for many polymers, but the same approach of encapsulation into silica nanoparticles can be used for cross-conjugated polymers similar to **P1** for which cooperative enhancement of σ^{TPA} values has been achieved.[42] Further, our approach can also be extended to oligomers[43] and other polymers,[44] hyperbranched polymers[45] and dendrimers[46] for which large nonlinearities are due to cooperative enhancement[9] rather than the additive effect of repeating units. Our results demonstrate that even when the polymer chains are constrained into a small volume in **P1**-NPS and **P1**-SNPs, there is no significant reduction of the optical nonlinearities due to possible bends of the polymer backbone or other polymer interactions or conformations. This is also supported by the data displayed in Fig. 2 which did not show any sign of reduction for the π-conjugation, *i.e.*, there is no blue shifting for the absorption peaks compared with those exhibited by the polymer in solution. Table 1 summarizes the nonlinear optical properties of our nanoparticles. In the following sections we demonstrate the utility of our nanoparticles for the imaging of cells through two-photon microscopy.

Photostability

Organic fluorophores usually suffer from irreversible photobleaching upon intense light irradiation due to photochemical reactions. Photobleaching is a drawback of organic fluorophores used in fluorescence microscopy. To evaluate how the formation of nanoparticles prevents this effect we compared the photostability of aqueous suspension of nanoparticles with the photostability of molecular solutions of **M1** and **P1**. To carry out this study, quartz cells of $0.1 \times 1 \times 4$ cm^3 were filled with **M1(P1)**-THF, **M1(P1)**-NPS and **M1(P1)**-SNPs and exposed to the illumination from a 150 watts Xenon lamp. The peak of absorption for each sample corresponding to the π–π* transition was then monitored over different intervals of time. Fig. 6 illustrates the relative photobleaching of the samples. In this figure both **M1**-THF and **P1**-THF exhibit low photostability *i.e.*, their absorbance decreased to approximately 50% of the initial value during the period of time chosen for light irradiation. Meanwhile, the decrease of absorption was less than 10% for all aqueous suspensions of nanoparticles, with the exception of **P1**-SNPs in which the photobleaching reached a maximum value of 13%. This demonstrates that the formation of nanoparticles prevents the photobleaching effect. We assign this effect to the isolation of the fluorescent materials from the medium. Photobleaching is often caused by molecular oxygen dissolved in the liquid medium that generates photo-oxidation reaction in

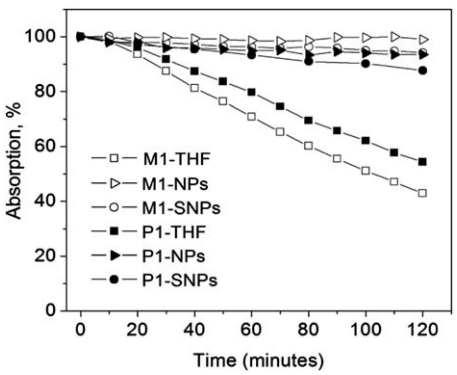

Fig. 6 Photostability of **M1** and **P1** in THF solutions and aqueous suspensions of nanoparticles. The samples were exposed to illumination from a Xenon lamp and the absorption at the peak of the π–π* transition was measured as a function of exposition time.

dyes. When **M1** (or **P1**) is encapsulated within the silica matrix, the reaction with oxygen is significantly hindered. Similarly, the molecular aggregation of **M1** and **P1** and the subsequent covering with surfactant micelles can effectively exclude oxygen outside **M1**-NPs and **P1**-NPs. Such reduction in the photobleaching effect is very useful for long time bio-imaging.

Cytotoxicity

In vitro cytotoxicity of nanoparticles and silica-loaded nanoparticles in A549 and HeLa cells was investigated by MTT assay. All tests were performed using suspensions with different concentration of nanoparticles (see Fig. 7). First, we compared the toxicity of nanoparticles stabilized with CTAB and Triton X-100, that is, **M1(P1)**-NP-CTAB and **M1(P1)**-NPs TRITON, finding that at concentrations of 7.5×10^{-5} M for **M1** and 4.1×10^{-7} M for **P1**, respectively (denoted in the figure as no dilution), there is no cell viability. In the case of **M1(P1)**-NP-TRITON, viabilities higher than 50% can be achieved in A549 and HeLa cells after 1 : 4 and 1 : 32 dilutions of the suspensions, respectively, while in the case of **M1(P1)**-NP-CTAB lower viabilities were observed even after more dilutions, in particular for HeLa cells. The low viability of **M1(P1)** nanoparticles synthesized through the reprecipitation method either with the use of CTAB or TRITON was substantially improved in silica nanoparticles loaded with **M1** or **P1**. For instance, Fig. 7a shows that at relatively high concentrations (1 : 1 dilutions) of 5.2×10^{-5} M and 3.1×10^{-7} M for **M1**-SNPs and **P1**-SNPs, respectively, the viability of A549 cells is approximately 80%, which is higher than that of **M1(P1)**-NP-CTAB and **M1(P1)**-NP-TRITON. Similarly, Fig. 7b shows how the viability is also improved in HeLa cells through the use of loaded silica nanoparticles, although in this case viabilities higher 80% are obtained in 1 : 8 dilutions. These results provide clear evidence of the importance of encapsulating the TPA materials in order to reduce their cytotoxicity.

Fluorescence microscopy

One-photon and two-photon fluorescence microscopies were used to study the uptake of all samples under study. For example, Fig. 8 displays micrographs of HeLa cells treated with **P1**-NPs and **P1**-SNPs as fluorescent probes and Hoechst 33258 to stain specifically the nucleus of cells. For the case of one-photon excitation the cells were illuminated at a wavelength of 488 nm (micrographs in the first and third row) while 740 nm was used for two-photon illumination (micrographs in the second and fourth row). For clarity, the images were taken with green and blue filters to identify nanoparticles (left column) and nucleus (middle column), respectively. The column at the right is the overlay of both images. Notice that under

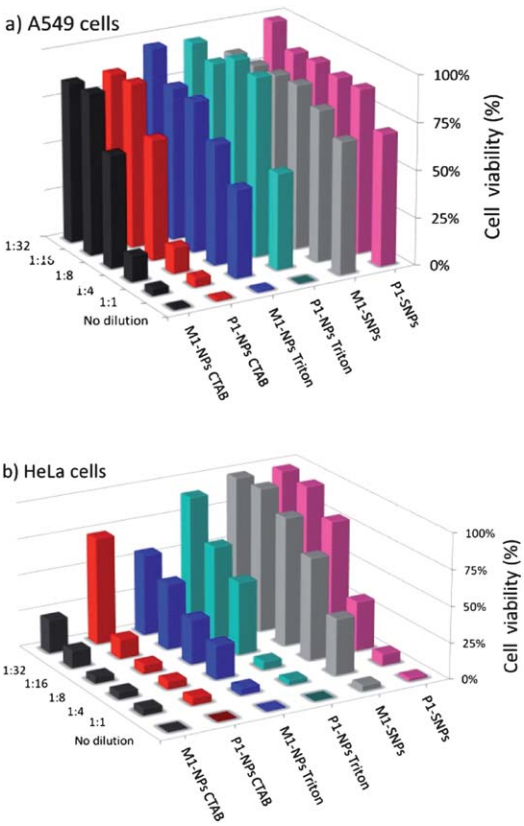

Fig. 7 Viability of (a) A546 cells and (b) HeLa cells cultured after the addition of aqueous suspensions at different dilutions of **M1(PI)**-NPs (stabilized with surfactants such as CTAB and Triton X-100) and **M1(P1)**-SNPs. The concentrations of suspensions before dilution were 7.5×10^{-5} M (**M1**-NPs), 4.1×10^{-7} M (**P1**-NPs), 5.2×10^{-5} M (**M1**-SNPs) and 3.1×10^{-7} M (**P1**-SNPs).

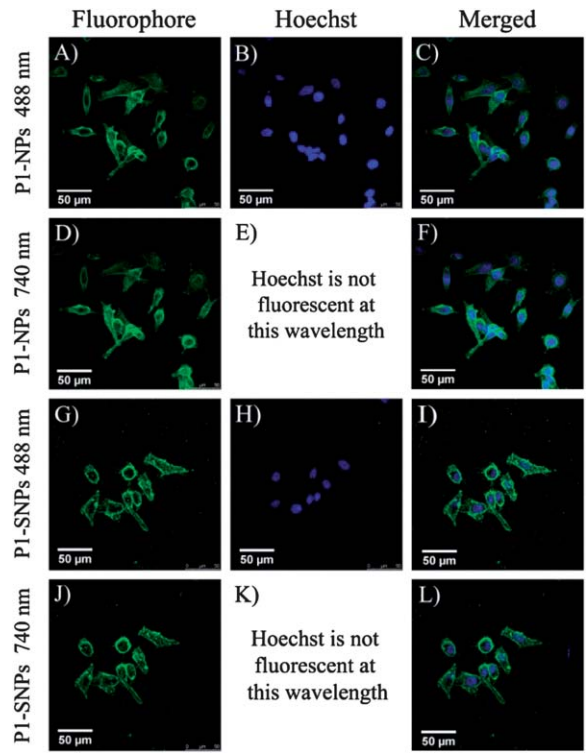

Fig. 8 One-photon (first and third row) and two-photon (second and fourth row) fluorescence images of HeLa cells treated with Hoechst 33258 and **P1**-NPs (A, B, C, D, and F) and **P1**-SNPs (G, H, I, J, and L). Left column: images taken with green filter to identify cytoplasm stained by nanoparticles under test. Middle column: the images taken with blue filter. Right column: superposition of images from the left and middle column. The wavelengths for one- and two-photon excitation are indicated to the left of the columns.

illumination at 740 nm the nucleus of cells (micrographs E and K) is not detected due to the poor two-photon activity of Hoechst 33258 at such a wavelength. Fig. 8 shows clearly that **P1**-NPs (micrographs A, B, C, D and F) and **P1**-SNPs (micrographs G, H, I, J and L) penetrated into the cells and reversibly stained the cytoplasm, without specific binding to cellular components. This was expected, since for the particular case of **P1**-SNPs no specific treatment was followed after silica encapsulation to conjugate the nanoparticle surface. Similar micrographs were obtained from cells treated with nanoparticles synthesized from **M1** but with the use of suspensions with larger concentrations due to the lower two-photon activity of such samples.

Conclusions

We made a comparative study of the two-photon action from a fluorene-based monomer and its polymer when they were molecularly dissolved, agglomerated in nanoparticles and encapsulated into silica nanoparticles. In particular, the polymer-doped silica nanoparticles gave high nonlinearities, on the order of 10^3 GM, excellent quantum yields with good photostability and viability; these properties were exploited to obtain two-photon fluorescence micrographs of HeLa cells. The doped silica nanoparticles studied here are attractive for their application in two-photon bioimaging and can be extended to other potential application in biosensing and assay labeling. To the best of our knowledge, this is the first time that polymer-doped silica nanoparticles have been fully characterized for their TPA and TPEF properties.

Acknowledgements

This work was partially supported by CONACyT (Grants 132946, 151842, 152971) and from DGAPA-UNAM (PAPIIT IN 104211). The authors thank Martin Olmos for technical assistance and M. C. Iván José Galván Mendoza, manager of the Confocal and Multiphoton microscopy Unit, Central Labs, CINVESTAV-IPN.

Notes and references

1 W. Denk, J. H. Strickler and W. W. Webb, *Science*, 1990, **248**, 73.
2 J. E. Ehrlich, X. L. Wu, I.-Y. S. Lee, Z.-Y. Hu, H. Röckel, S. R. Marder and J. W. Perry, *Opt. Lett.*, 1997, **22**, 1843–1845.
3 P. Wei, O. F. Tan, Y. Zhu and G. H. Duan, *Appl. Opt.*, 2007, **46**, 3694–3699.
4 N. S. Makarov, A. Rebane, M. Drobizhev, H. Wolleb and H. Spahni, *J. Opt. Soc. Am. B*, 2007, **24**, 1874–1885.
5 S. Kim, T. Y. Ohulchanskyy, H. E. Pudavar, R. K. Pandey and P. N. Prasad, *J. Am. Chem. Soc.*, 2007, **129**, 2669–2675.
6 P. T. C. So, C. Y. Dong, B. R. Masters and K. M. Berland, *Annu. Rev. Biomed. Eng.*, 2000, **2**, 399–429.
7 C. Xu and W. W. Webb, *J. Opt. Soc. Am. B*, 1996, **13**, 481–491.
8 H. M. Kimw and B. R. Cho, *Chem. Commun.*, 2009, 153–164.
9 G. S. He, L.-S. Tan, Q. Zheng and P. N. Prasad, *Chem. Rev.*, 2008, **108**, 1245–1330.
10 S. Kim, Q. Zheng, G. S. He, D. J. Bharali, H. E. Pudavar, A. Baev and P. N. Prasad, *Adv. Funct. Mater.*, 2006, **16**, 2317–2323.
11 Y. Tian, C.-Y. Chen, Y.-J. Cheng, A. C. Young, N. M. Tucker and A. K.-Y. Jen, *Adv. Funct. Mater.*, 2007, **17**, 1691–1697.
12 Y. S. Zhao, H. Fu, A. Peng, Y. Ma, D. Xiao and J. Yao, *Adv. Mater.*, 2008, **20**, 2859–2876.
13 C. S. Yang, C. H. Chang, P. J. Tsai, W. Y. Chen, F. G. Tseng and L. W. Lo, *Anal. Chem.*, 2004, **76**, 4465–4471.
14 I. Miletto, A. Gilardino, P. Zamburlin, S. Dalmazzo, D. Lovisolo, G. Caputo, G. Viscardi and G. Martra, *Dyes Pigm.*, 2010, **84**, 121–127.
15 D. Knopp, D. Tang and R. Niessner, *Anal. Chim. Acta*, 2009, **647**, 14–30.
16 W.-B. Wu, C. Liu, M.-L. Wang, W. Huang, S.-R. Zhou, W. Jiang, Y.-M. Sun, Y.-P. Cui and C.-X. Xu, *J. Solid State Chem.*, 2009, **182**, 862–868.
17 P. Howes, M. Green, J. Levitt, K. Suhling and M. Hughes, *J. Am. Chem. Soc.*, 2010, **132**, 3989–3996.
18 J. Pecher and S. Mecking, *Chem. Rev.*, 2010, **110**, 6260–6279.
19 C. Wu, C. Szymanski and J. McNeill, *Langmuir*, 2006, **22**, 2956–2960.
20 S. W. Bae, W. Tan and J.-I. Hong, *Chem. Commun.*, 2012, **48**, 2270–2282.
21 J. L. Vivero-Escoto, R. C. Huxford-Phillips and W. Lin, *Chem. Soc. Rev.*, 2012, **41**, 2673–2685.
22 A. Schulz and C. McDonagh, *Soft Matter*, 2012, **8**, 2579–2585.
23 H. Tan, M. Wang, C.-T. Yang, S. Pant, K. K. Bhakoo, S. Y. Wong, Z.-K. Chen, X. Li and J. Wang, *Chem.–Eur. J.*, 2011, **17**, 6696–6706.
24 S. Beaupre, P.-L. T. Boudreault and M. Leclerc, *Adv. Mater.*, 2010, **22**, E6–E27.
25 W. Tang, L. Ke, L. Tan, T. Lin, T. Kietzke and Z.-K. Chen, *Macromolecules*, 2007, **40**, 6164.
26 T.-C. Lin, Y.-H. Lee, C.-L. Hu, Y.-K. Li and Y.-J. Huang, *Eur. J. Org. Chem.*, 2012, 1737–1745.
27 D. S. Correa, L. De Boni, B. Nowacki, I. Grova, B. D. Fontes, P. C. Rodrigues, J. R. Tozoni, L. Akcelrud and C. R. Mendonc, *J. Polym. Sci., Part B: Polym. Phys.*, 2012, **50**, 148–153.
28 K. D. Belfield, M. V. Bondar, C. O. Yanez, F. E. Hernandez and O. V. Przhonska, *J. Mater. Chem.*, 2009, **19**, 7498–7502.
29 G. Ramos-Ortíz, J. L. Maldonado, M. C. G. Hernández, M. G. Zolotukhin, S. Fomine, N. Fröhlich, U. Scherf, F. Galbrechtc, E. Preis, M. Salmon, J. Cárdenas and M. I. Chávez, *Polymer*, 2010, **51**, 2351–2359.
30 T. Yanaia, D. P. Tewb and N. C. Handy, *Chem. Phys. Lett.*, 2004, **393**, 51–57.
31 M. J. Frisch, *et al.*, *Gaussian 09, Revision B.01*, Gaussian, Inc., Wallingford, CT, 2009.
32 X. Wang, S. Yao, H.-Y. Ahn, Y. Zhang, M. V. Bondar, J. A. Torres and K. D. Belfield, *Biomed. Opt. Express*, 2010, **1**, 453–462.
33 J. Qian, A. Gharibi and S. He, *J. Biomed. Opt.*, 2009, **14**, 014012.
34 F. J. Arriagada and K. Osseo-Asare, *J. Colloid Interface Sci.*, 1995, **170**, 8–17.

35 M. A. Albota, C. Xu and W. W. Webb, *Appl. Opt.*, 1998, **37**, 7352.
36 N. S. Makarov, M. Drobizhev and A. Rebane, *Opt. Express*, 2008, **16**, 4029.
37 V. Lebret, L. Raehm, J.-O. Durand, M. Smaïhi, C. Gérardin, N. Nerambourg, M. H. V. Werts and M. Blanchard-Desce, *Chem. Mater.*, 2008, **20**, 2174–2183.
38 A. P. Kulkarni, X. Kong and S. A. Jenekhe, *J. Phys. Chem. B*, 2004, **108**, 8689–8701.
39 C. D. Andrade, C. O. Yanez, L. Rodriguez and K. D. Belfield, *J. Org. Chem.*, 2010, **75**, 3975–3982.
40 W.-C. Wu, C.-Y. Chen, Y. Tian, S.-H. Jang, Y. Hong, Y. Liu, R. Hu, B. Z. Tang, Y.-T. Lee, C.-T. Chen, W.-C. Chen and A. K.-Y. Jen, *Adv. Funct. Mater.*, 2010, **20**, 1–11.
41 E. Chelebaeva, L. Raehm, J.-O. Durand, Y. Guari, J. Larionova, C. Guérin, A. Trifonov, M. Willinger, K. Thangavel, A. Lascialfari, O. Mongin, Y. Mir and M. Blanchard-Desce, *J. Mater. Chem.*, 2010, **20**, 1877–1884.
42 X. Li, X. Zhang, W. Li, Y. Wang, T. Liu, B. Zhang and W. Yang, *J. Mater. Chem.*, 2011, **21**, 3916–3924.
43 B. R. Cho, M. J. Piao, K. H. Son, S. H. Lee, S. J. Yoon, S.-J. Jeon and M. Cho, *Chem.–Eur. J.*, 2002, **8**, 3916–3924.
44 W. Yao-Chuan, Y. Yong-Li, Z. Hui, H. Nan, F. Miao, Q. Shi-Xiong and C. Yu, *Acta Phys.-Chim. Sin.*, 2010, **26**, 707–713.
45 Y. Jiang, Y. Wang, J. Hua, S. Qu, S. Qian and H. Tian, *J. Polym. Sci., Part A: Polym. Chem.*, 2009, **47**, 7400–7408.
46 O. Varnavski, X. Yan, O. Mongin, M. Blanchard-Desce and T. Goodson, III, *J. Phys. Chem. C*, 2007, **111**, 149–162.